

Control of stochastic multistable systems: Experimental demonstration

B. K. Goswami,¹ S. Euzzor,² K. Al Naimee,² A. Geltrude,² R. Meucci,² and F. T. Arecchi²
¹*Laser and Plasma Technology Division, Bhabha Atomic Research Centre, Mumbai 400085, India*
²*Istituto Nazionale di Ottica Applicata, 50125 Florence, Italy*

(Received 23 March 2009; revised manuscript received 27 May 2009; published 22 July 2009)

Stochastic disturbances and spikes (sudden sharp fluctuations of any system parameter), commonly observed among natural and laboratory-scale systems, can perturb the multistable dynamics significantly and become a serious impediment when the device is designed for a certain dynamical behavior. We experimentally demonstrate that suitable periodic modulation of any system parameter may efficiently control such stochastic multistability related problems. The control mechanism is verified individually with two standard models (namely, an analog circuit of Lorenz equations and a cavity-loss modulated CO₂ laser), against three externally introduced disturbing signals, (namely, white Gaussian noise, pink noise, and train of spikes). Indeed, with both the systems, it has been observed that the modulation is capable to significantly control untoward jumps to coexisting attractors that otherwise would have occurred due to either of the disturbances. These results establish the robustness and wide applicability of this control mechanism in resolving stochastic multistability related problems.

DOI: [10.1103/PhysRevE.80.016211](https://doi.org/10.1103/PhysRevE.80.016211)

PACS number(s): 05.45.-a, 05.40.Ca, 07.50.Ek, 47.52.+j

Stochastic disturbances, commonly observed among natural and laboratory-scale systems, can influence the multistable dynamics in many ways [1–3]. For instance, it may lead to (i) unidirectional transitions from smaller basins of attraction to relatively larger basins, (ii) intermittent transitions among coexisting attractors (“multistate hopping intermittency”) for relatively stronger noise, (iii) stochastic resonance [4] and (iv) advancement of local bifurcations (or crises), intermittent shuttling over the respective bifurcation (or crisis) criticality and coherence resonance [5] (also observable in the monostable scenario).

In general, from the viewpoint of designed performance of any applications, multistability in the presence of stochastic disturbance is undesirable if the device has to remain at any given attractor. While examples of such systems (applications) are many [6,7], we mention here about the natural circulation fluid dynamical systems, for instance, the coolant flow in the nuclear reactor based power generators that are topical subjects of research [8,9]. While designing the operating regimes of the coolant circulatory systems, it is preferable to avoid oscillatory instabilities. Therefore, the experimental observation of multistability in such thermal hydraulic systems [8] recommends a precautionary measure to avoid any stochastic perturbation induced settlement to such oscillatory convective flow patterns.

Let us refer to some well-known concepts of controlling multistable systems. In noise and feedback control, the noise helps to bring the system in the close proximity of the desired basin when the feedback control is applied to stabilize the system at a specified attractor [10] or to repel from another [11]. A relatively faster control technique incorporates targeting the desired attractor [12]. However, all these feedback based control mechanisms have certain limitations toward wider and reproducible applications. They require, in the words of Feudel [7], “an appropriate feedback-loop as well as a permanent tracking of the trajectory” that may not be an easy proposition in general.

In contrast, the periodic perturbation control mechanism, in the form of modulation of any system parameter [13] or

introduction of a driving force [14], is easily realizable, purely deterministic, and therefore reliably reproducible. The control mechanism has been theoretically demonstrated with a few nonstochastic models of laboratory-scale systems, for instance, delayed feedback CO₂ [15] and semiconductor [16] lasers, and Lorenz equations [17]. The periodic perturbation makes the undesirable attractor chaotic and simultaneously transforms the invariant manifolds of the neighboring boundary saddle, leading to homoclinic tangency and boundary crisis of the chaotic attractor. This control technique has also been shown to transform an exceedingly complex multistable scenario (simultaneous coexistence of infinitely many attractors that occur in the weak dissipative limit [18]) to a monostable one [19]. From the experimental side, the periodic perturbation mechanism has been validated so far with systems having such excellent signal-to-noise ratio. For instance, CO₂ [13] and fiber lasers [20] and an analog circuit of Lorenz equations [17].

Keeping in mind other laboratory-scale or natural systems where stochastic disturbances or sudden sharp fluctuations in system parameters are commonly observed, it might be interesting to know whether the control perturbation is equally capable to handle various types and strengths of stochastic disturbances. In the case of Hénon map [19], the control has been theoretically shown to work in the presence of Gaussian white noise. Furthermore, similar theory, individually with Lorenz equations and Toda oscillator, predict the successful applicability even in the presence of strong noise [14]. However, to our knowledge, so far no significant experimental verification has been made toward controlling stochastic multistability. This motivates us to experimentally validate the control technique with two standard models, namely, an analog circuit of Lorenz equations (the paradigm of thermal hydraulics) and a cavity-loss modulated CO₂ laser (the most well-known experimental prototype of nonlinear systems). Also, the control mechanism is tested against three types of disturbing sources, namely, white Gaussian noise, pink noise, and a train of spikes (or sharp trigger pulses). The analog circuit dynamics is perturbed individually with white or pink

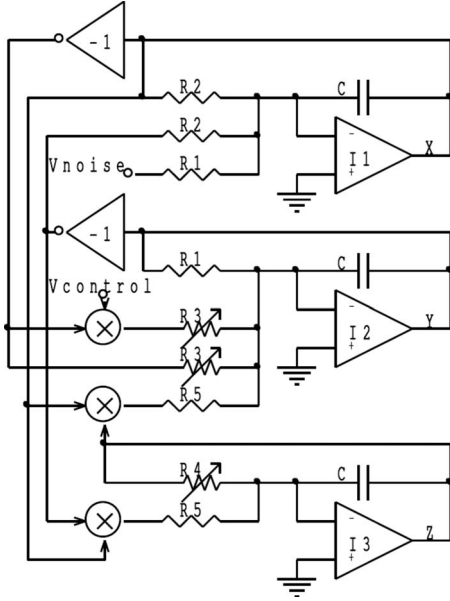


FIG. 1. Analog circuit of stochastic Lorenz equations under periodic parameter modulation.

noise. Indeed, on both occasions, it is observed that the periodic parameter modulation is capable to control untoward jumps to coexisting attractors that otherwise would have occurred due to the presence of the disturbing sources. Furthermore, similar efficacy of the control mechanism has also been observed when the multistable CO_2 laser is disturbed individually with a train of spikes or white noise. First the experiments with the analog circuit are explained in more detail.

The schematic of the analog circuit of Lorenz equations is shown in Fig. 1 and the voltage kinetics is defined by

$$\begin{aligned}\dot{X} &= -\frac{1}{R_2 C}(X - Y) - \frac{V_{noise}}{R_1 C}, \\ \dot{Y} &= \frac{(1 + V_{control})}{R_3 C}X - \frac{1}{R_1 C}Y - \frac{1}{R_5 C}XZ, \\ \dot{Z} &= \frac{1}{R_5 C}XY - \frac{1}{R_4 C}Z,\end{aligned}$$

where $R_1 = 75 \text{ k}\Omega$, $R_2 = 7.5 \text{ k}\Omega$, $R_3 = 2.89 \text{ k}\Omega$, $R_4 = 28.125 \text{ k}\Omega$, $R_5 = 30 \text{ k}\Omega$, and $C = 6.8 \text{ nF}$. We have used LT1114 operational amplifier ICs for analog integrations (denoted by I1, I2, and I3) and inversions (denoted by “-1”), and MLT04 ICs for analog multiplications (denoted by cross symbols inside circles). The noise generator is shown by V_{noise} and the periodic control modulation by $V_{control} = A \sin(2\pi\nu t)$. In the absence of noise and control signals, the circuit equations can be transformed to Lorenz equations with $\sigma = 10$, $\rho = 25.95$, $\beta = 8/3$. For $2.87 \text{ k}\Omega < R_3 < 2.91 \text{ k}\Omega$, the circuit exhibits simultaneous coexistence of the chaotic attractor and two stable steady states, denoted by S_+ (for $X > 0$) and S_- (for $X < 0$). The operating point $R_3 = 2.89 \text{ k}\Omega$ is inside the multistable regime. The basin of each

steady state is determined by the surrounding unstable periodic orbit (UPO). The control of noise-free multistable Lorenz model has been studied theoretically and experimentally in Ref. [17] that we review here in few lines. By suitably choosing the control amplitude and frequency, the chaotic attractor can be destroyed by introducing collision with any UPOs so that the circuit jumps to a steady state. If the control frequency is close to the UPO frequency, the threshold control amplitude, required to induce such boundary crisis, would be minimum. This phenomenon has been referred to as crisis resonance. In the experiments with the present circuit, we have observed similar destruction of chaotic attractor by the periodic modulation of system parameters. The curve in Fig. 2(a) shows the crisis threshold control amplitude (A_{min}) at various control frequencies. The threshold amplitude is minimal when the control frequency is close to 400 Hz and 1.6 kHz. With this information about the noise-free case, we now introduce white noise to the circuit while the control is switched off. Figures 2(b) and 2(c) illustrate some statistical features of the white noise generator. One million time-series data of noise (sampling period $20 \mu\text{s}$) have been used for such analysis. Figure 2(b) shows that the noise magnitude lies in the range $[-6.5 \text{ V}; 6.5 \text{ V}]$ that represents strong noise as the absolute magnitudes of X , Y and Z lie in general within 3 V. The entire range of noise magnitude has been divided into 25 intervals and the probability distribution over these intervals has been computed and illustrated by filled circles. The solid line in this plot denotes the Gaussian fit with standard deviation 2.55 V and zero mean. Figure 2(c) demonstrates the corresponding uniform broadband Fourier spectrum. We analyze the dynamics in the phase space of such strong noise-driven circuit. A suitably large region in the phase space ($-1.5 < X < 1.5$, $0 < Z < 3$) is selected around the chaotic attractor and the stable steady states. This phase-space region is uniformly divided into ($N_1 = 25 \times 25$) cells. We record the time series of X and Z voltages for suitably large time-interval, say $N_2 = 10^6$ time steps (each of 20 microseconds duration), and compute the total number of visits in each cell. The occupation probability density $D(X, Z)$ per unit cell around the point (X, Z) is defined by $D(X, Z) = P(X, Z) / (N_1 N_2)$ where $P(X, Z)$ denotes the number of time steps the system remains inside the cell around (X, Z) point. While comparing the probability distribution of the uncontrolled noisy dynamics [Fig. 2(d)] with that of the controlled scenario [Fig. 2(e)], we keep the values of N_1 and N_2 unchanged. The probability distribution [for convenience, represented by $P(X, Z)$] in Fig. 2(d) vividly reveals the stochastically driven motion in the basin of the chaotic attractor. In particular, the system stays maximum probable period around the saddle ($X = Y = Z = 0$). This feature can be explained as follows: the speed of convergence to the saddle via stable manifold or divergence away from the saddle via unstable manifold decreases substantially in the vicinity of the saddle resulting in the sharp increase of the occupation probability. However, away from the saddle, the system moves relatively fast inside the basin of the chaotic attractor, including occasional spiraling around the UPOs, before approaching back again to the saddle via the stable manifold. The prominent two holes in the probability distribution profile indicate that the system rarely stays inside the

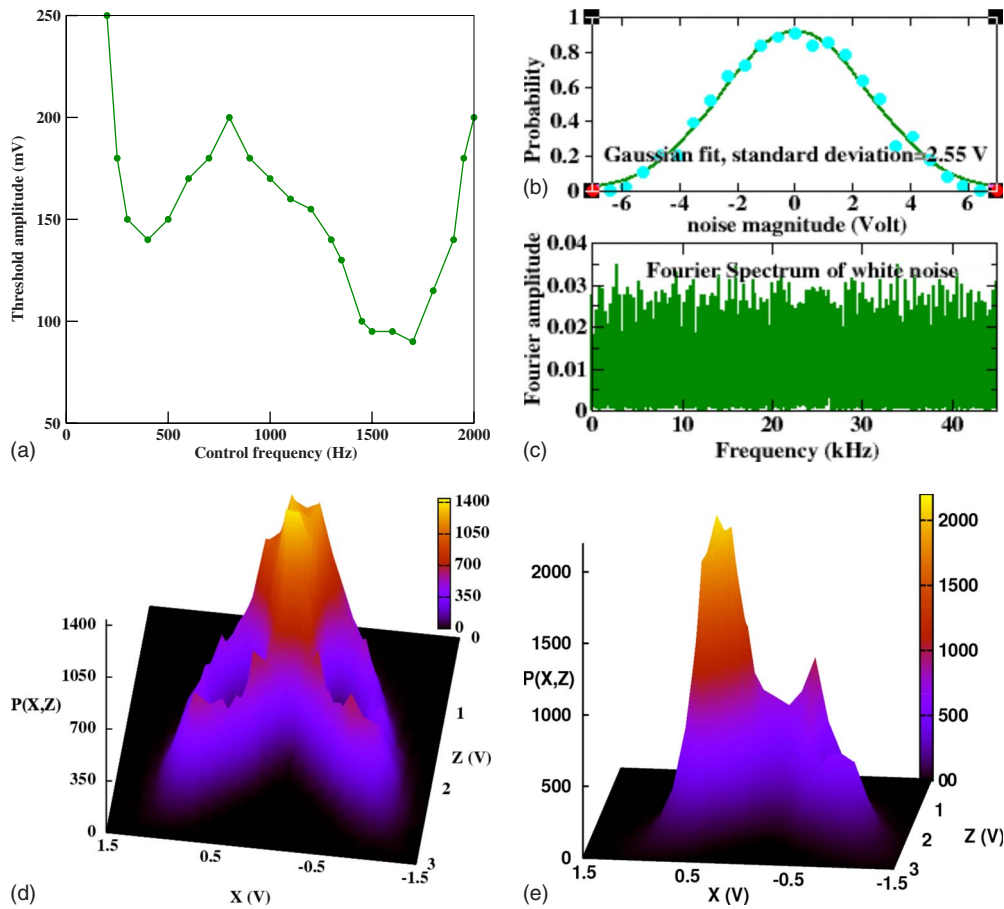


FIG. 2. (Color online) (a) Threshold control amplitude (A_{\min}) versus control frequency (ν), shown by star symbols. (b) Probability distribution of the white noise: experimental data are shown by filled circle symbols and the corresponding Gaussian fit by solid line. (c) Fourier spectrum of white noise. (d) and (e) represent the probability distributions for the uncontrolled noisy and controlled noisy circuits, respectively. (d) Without control, probability is highest around the saddle ($X=Y=Z=0$) inside the chaotic attractor and negligible in the basins of steady-state attractors. (e) However, in the presence of control modulation, the circuit dynamics is essentially confined around one steady state while the occupation probability in the chaotic attractor exhibits a sharp decrease.

basins of steady states. If the system ever enters any such basin, noise is strong enough to eject the system very fast and put it back inside the chaotic attractor.

Such a scenario can also be changed remarkably when the control modulation is switched on with appropriately set parameter values. Figure 2(e) demonstrates such a case. The control frequency is set at $\nu=1.70$ kHz where the crisis threshold amplitude is minimum. Also, the control amplitude is set at ($A_c=200$ mV), higher than the crisis threshold. The phase-space probability distribution demonstrates a completely contrasting scenario with respect to the uncontrolled case. The probability density around the steady state S_+ is now much larger than that around the chaotic attractor in general and the saddle in particular. The underlying phenomenon behind such significant transformation is the control perturbation induced boundary crisis of the chaotic attractor. In particular, the sharp reduction of occupation period around the saddle ($X=Y=Z=0$) is a consequence of a homoclinic tangency. This is because the system is driven away by noise whenever the trajectory is close to any tangency points and therefore the system does not get adequate opportunity to approach the saddle.

Next we analyze the effect of control modulation in the

presence of pink noise. Figure 3(a) shows a typical time series that clearly suggests rare occurrence of small-amplitude noise. Figure 3(b) describes the corresponding (grossly) symmetric probability distribution with the minimum at the center and the most probable magnitude (absolute value) of noise in the interval between 0.6 and 1 V. This is in contrast with Gaussian white noise. Besides, the Fourier spectrum in Fig. 3(c) shows a maximum in the low frequency range and an overall decrease along the high frequency range. Thus the spectrum is also qualitatively different from that of white noise. We compute the phase-space occupation probability distribution in the same manner as followed in the case of white noise. The circuit dynamics is analyzed for $N_2=500\,000$ time steps. Figure 3(d) illustrates the probability distribution of the pink-noise induced circuit dynamics. It reveals that the circuit remains in the chaotic attractor. In particular, the probability is maximum around the saddle ($X=Y=Z=0$). Also, the occupation density is again minimum around the steady states. These features are similar with the white noise case. As we introduce the control modulation suitably, the situation changes drastically. Figure 3(e) shows the probability distribution in the presence of control modulation ($A_c=130$ mV; $\nu=1.7$ kHz). Notice-

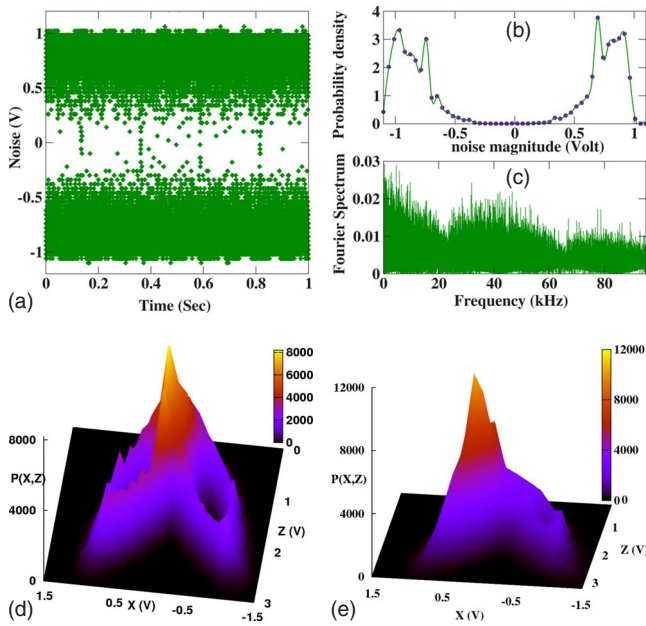


FIG. 3. (Color online) (a) Time series, (b) probability distribution, and (c) Fourier spectrum of pink noise. (d) and (e) represent the probability density of phase-space occupation for uncontrolled noisy and controlled noisy circuits respectively. (d) Without control, probability is highest around the saddle ($X=Y=Z=0$) and negligible in the basins of the steady-state attractors. (e) In the presence control modulation, one steady state becomes most preferred attractor while the occupation density has sharply reduced in the chaotic attractor.

ably the scenario is again completely contrasting to the uncontrolled case. $P(X,Z)$ is maximum around “ S_+ ” steady state. In contrast, inside the chaotic attractor, in particular, around the saddle, it has predominantly gone down. Thus, we have demonstrated control of stochastic multistable scenario quite successfully with two different types of stochastic disturbances.

Here we explore the effect of periodic parameter modulation on the stochastic multistable scenario of a single-axial mode TEM₀₀ CO₂ laser. Figure 4 schematically illustrates the experimental setup of the laser where an electro-optic modulator (EOM) is inserted to create multistability. The cavity

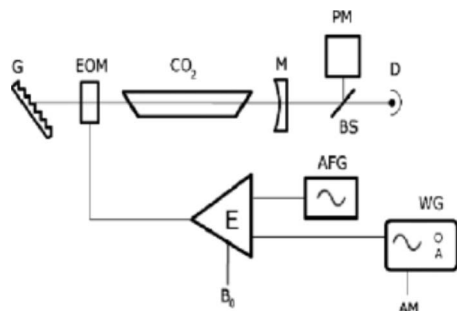


FIG. 4. The schematic of the CO₂ laser: CO₂ Gas mixture tube (CO₂), grating (G), mirror (M), Beam-splitter (BS), photodetector (D), laser power meter (PM), electro-optic modulator (EOM), wave generator (WG), arbitrary function generator (AFG), and differential amplifier (E).

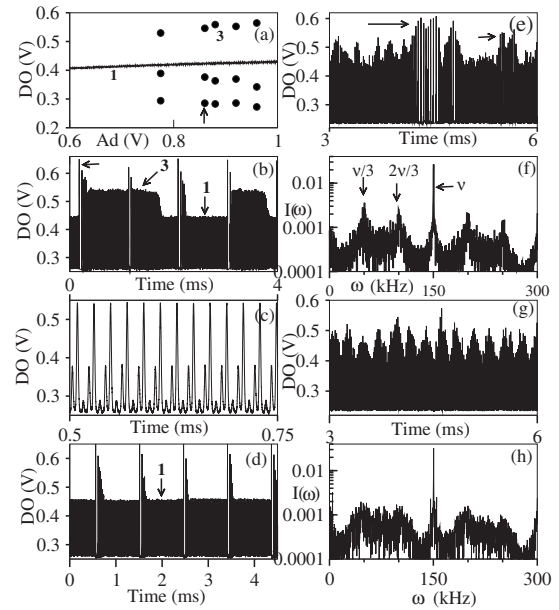


FIG. 5. (a) Bifurcation diagram [laser intensity (DO) versus modulation amplitude (Ad)] shows the period-3 branch (filled symbols) coexisting with the period-1 branch (solid line). (b) The intensity time series illustrates trigger-induced transitions from period-1 to period-3. (c) The period-3 time series is shown with better resolution. (d) Successful inhibition of the trigger-induced switching by a control signal. Panels (e) and (f), respectively, show the laser intensity time series and its FFT when the laser is driven by Gaussian white noise signal (80 mVpp). Two period-3 bursts are shown by horizontal arrows in panel (e). (f) The presence of spectral lines of frequency $\nu/3$ and its higher harmonics in the FFT also indicate noise-induced jumps between period-1 and period-3. Panels (g) and (h) demonstrate, respectively, the intensity time series and its FFT in the additional presence of the control modulation (4 kHz frequency and 70 mVpp). (g) The intensity time series does not exhibit any prominent period-3 bursting. (h) The spectrum also does not exhibit any prominent spectral lines of the period-3 attractor.

length (L) is 1.45 m and the total transmission T is approximately 0.10 per cavity roundtrip. The cavity decay rate of the laser intensity can be expressed as $k(t) = k_0(1 + \alpha \sin^2(\pi/V_\lambda)[B_0 + M F(t)])$; $k_0 = cT/L$, c being the speed of light in the vacuum, $\alpha = (1 - 2T)/2T$. $V_\lambda = 2650T$ is the half-wave voltage and B_0 is the bias voltage. The time-varying signal $F(t)$, amplified M times, and the bias voltage, B_0 are added, before being applied to the EOM. For our experiments, laser power is 30 mW, $M = 85$ and $B_0 = 365$ V. The laser intensity is measured in terms of the photodetector output voltage (DO), visually analyzed by an oscilloscope and corresponding data are stored in a computer for further time-series analysis and fast Fourier transform (FFT).

The relaxation oscillation frequency, as measured by probing the harmonic resonance, is approximately 50 kHz. We drive the EOM by a periodic voltage of frequency ν and amplitude Ad (provided by the AFG) where the drive frequency is three times the relaxation oscillation frequency ($\nu = 150$ kHz). In this period-3 subharmonic resonance region, we observe coexistence of period-3 attractor with the period-1 attractor. Panel (a) in Fig. 5 shows the bifurcation diagram (laser intensity versus modulation amplitude) where

the vertical coordinate represents the stroboscopically sampled photodetector output signal (DO); the sampling frequency is equal to the modulation frequency. The solid line denotes the period-1 branch and the filled symbols denote the period-3 branch. We fix the operating point at the drive amplitude 860 mV, indicated by an arrow. Next with the help of AFG, we add a train of trigger pulses (of repetition rate 1 kHz) over the previous periodic signal. The phase difference and pulse heights are adjusted appropriately so that the laser jumps from the period-1 to period-3 attractors. The trigger pulses in these experiments symbolize sharp spurious fluctuations that may occur due to many reasons and are commonly observed in laser electronics. The intensity time series in panel (b) illustrates a few trigger-induced transitions from period-1 to period-3; one is shown by a horizontal arrow. The period-3 state is denoted by “3” and period-1 by “1.” The period-3 time series is shown with better resolution in panel (c). The objective of the control mechanism is to counter the jumps to period-3 and confine the laser at the period-1 attractor. We additionally introduce the control modulation, provided by the wave generator (WG). By keeping the control frequency fixed and increasing the control amplitude, we indeed observe a fascinating qualitative change in the laser dynamics. Panel (d) shows the intensity time series of such a case with control frequency 30 kHz and amplitude 10 mV. By comparing with the uncontrolled scenario, shown in panel (b), one may notice successful inhibition of the trigger-induced switching from period-1 to period-3 attractors. The laser remains predominantly in the period-1 attractor in spite of recurrent train of trigger pulses. This is because the period-3 attractor is destroyed by the control modulation and the basin has lost the capacity to retain the system even if any trigger pulses send the system there.

Next, we investigate the control of white Gaussian noise-driven multistable scenario by introducing Gaussian white noise source in place of the trigger pulse generator. The noise generator is not shown explicitly in the schematic. We increase the strength of the noise signal sufficiently so that the laser exhibits intermittent jumps to period-3 basin. Panels (e) and (f), respectively, show the noise-driven laser intensity time series and its FFT for the noise strength 80 mVpp. Two period-3 bursts are shown by horizontal arrows in panel (e). The noise-induced jumps to period-3 attractor are also evident in the FFT [panel (e)] where one may notice the presence of spectral line of frequency $\nu/3$ and its higher harmonics. Next a slow periodic control modulation (of frequency 4 kHz) is introduced by the WG and the control amplitude is increased. Here again, we notice successful control of switching to the period-3 attractor for control amplitude 70 mVpp and above. Panel (g) shows the intensity time series that, in contrast with the uncontrolled scenario in panel (e), does not exhibit any prominent period-3 bursting. The peri-

odic envelope modulation, in panel (g), is due to the 4 kHz control modulation. The inhibition of visits to the period-3 basin is also reflected in the intensity FFT, shown in panel (h). Unlike the uncontrolled scenario [panel (f)], the spectrum does not exhibit any spectral line of the period-3 attractor. Thus from the laser experiments, we have demonstrated the successful control of stochastic multistability individually in the presence two types of disturbing environment-sharp triggers and white noise. One reason of such magnificent success of the control mechanism could be the fact that noise does not deter crisis. On the contrary, noise may advance the onset of such crisis [21].

Finally, we may also note that in the presence of the control perturbation, all attractors and their basins are affected. Commonly the strongest attractor undergoes interior crisis at very large control amplitude while the remaining attractors undergo boundary crisis at much less values of the control amplitude. It may therefore be possible to compute a sequential hierarchy of threshold control amplitudes corresponding to crises of the coexisting attractors. By limiting the control parameter magnitudes appropriately, it may be feasible to leave the strongest attractor essentially unperturbed while destroy the remaining ones. Therefore, this control mechanism relies on the “survival of the fittest” concept and is very efficient in selecting the strongest attractor. This has been observed so far that the attractors that resemble the corresponding linear or regular systems are the strongest. For instance, in the case of any periodically forced nonlinear system, the period-1 attractor is the strongest. Similarly, in the case of autonomous systems, the steady states are the strongest. These features have been recently found in the case of Hénon map [19], Toda oscillator, and Lorenz equations [14]. Therefore, this control mechanism could be very effective to confine the stochastic multistable dynamics around the linear (or regular) regimes.

To conclude, we have experimentally demonstrated the control of stochastic multistability, by periodic perturbation mechanism, individually with an analog circuit of Lorenz equations and a CO₂ laser. In the case of the analog circuit, we have tested the control mechanism individually under two contrasting types of externally controlled noise sources, namely, white Gaussian noise and pink noise. In the case of the CO₂ laser, we have done similar experiments individually in the presence of an array of trigger pulses and Gaussian white noise. Remarkably, on all occasions, the control mechanism works successfully. These results strongly endorse the robustness and wide applicability of this control mechanism in resolving stochastic multistability related problems.

This work is supported by the Department of Atomic Energy, Government of India (Grant No. 11-R&D-BAR-4.11-0200: XI-N-R&D-26.09). B.K.G. sincerely acknowledges the help of S. Brugioni and F. Salvadori.

- [1] S. Kraut, U. Feudel, and C. Grebogi, *Phys. Rev. E* **59**, 5253 (1999).
- [2] S. Kraut and U. Feudel, *Phys. Rev. E* **66**, 015207(R) (2002).
- [3] C. Masoller, *Phys. Rev. Lett.* **88**, 034102 (2002).
- [4] L. Gammaitoni, P. Hanggi, P. Jung, and F. Marchesoni, *Rev. Mod. Phys.* **70**, 223 (1998).
- [5] A. S. Pikovsky and J. Kurths, *Phys. Rev. Lett.* **78**, 775 (1997); D. E. Postnov, S. K. Han, T. G. Yim, and O. V. Sosnovtseva, *Phys. Rev. E* **59**, R3791 (1999).
- [6] B. K. Goswami and A. N. Pisarchik, *Int. J. Bifurcation Chaos Appl. Sci. Eng.* **18**, 1645 (2008).
- [7] U. Feudel, *Int. J. Bifurcation Chaos Appl. Sci.* **18**, 1607 (2008).
- [8] W. L. Chen, S. B. Wang, S. S. Twu, C. R. Chung, and Chin Pan, *Int. J. Multiphase Flow* **27**, 171 (2001); J. D. Lee and Chin Pan, *Nucl. Eng. Des.* **235**, 2358 (2005); P. K. Vijayan, M. Sharma, and D. Saha, *Exp. Therm. Fluid Sci.* **31**, 925 (2007).
- [9] A. Manera, U. Rohde, H.-M. Prasser, and T. H. J. J. van der Hagen, *Nucl. Eng. Des.* **235**, 1517 (2005); M. Furuya, F. Inada, and T. H. J. J. van der Hagen, *ibid.* **235**, 1557 (2005); **235**, 1635 (2005).
- [10] L. Poon and C. Grebogi, *Phys. Rev. Lett.* **75**, 4023 (1995).
- [11] U. Feudel and C. Grebogi, *Chaos* **7**, 597 (1997).
- [12] Y.-C. Lai, *Phys. Lett. A* **221**, 375 (1996); Y.-C. Lai and C. Grebogi, *Phys. Rev. E* **54**, 4667 (1996); E. E. N. Macau and C. Grebogi, *ibid.* **59**, 4062 (1999).
- [13] A. N. Pisarchik and B. K. Goswami, *Phys. Rev. Lett.* **84**, 1423 (2000).
- [14] B. K. Goswami, *Phys. Rev. E* **78**, 066208 (2008).
- [15] A. N. Pisarchik and B. F. Kuntsevich, *IEEE J. Quantum Electron.* **38**, 1594 (2002).
- [16] B. E. Martínez-Zérega, A. N. Pisarchik, and L. Tsimring, *Phys. Lett. A* **318**, 102 (2003).
- [17] B. K. Goswami, *Phys. Rev. E* **76**, 016219 (2007).
- [18] B. K. Goswami, *Phys. Rev. E* **62**, 2068 (2000); B. K. Goswami and S. Basu, *ibid.* **65**, 036210 (2002).
- [19] B. K. Goswami and S. Basu, *Phys. Rev. E* **66**, 026214 (2002).
- [20] A. N. Pisarchik, Y. O. Barmenkov, and A. V. Kiryanov, *Phys. Rev. E* **68**, 066211 (2003).
- [21] J. C. Sommerer, E. Ott, and C. Grebogi, *Phys. Rev. A* **43**, 1754 (1991); J. C. Sommerer, W. L. Ditto, C. Grebogi, E. Ott, and M. L. Spano, *Phys. Rev. Lett.* **66**, 1947 (1991).